Desalination and Water Treatment
www.deswater.com
doi: 10.5004/dwt.2018.22422

118 (2018) 153–162
June

Adsorption of Cu(II) and methylene blue from aqueous solutions by magnetic humic acid nanoparticles

Rong Ping Chen[a], Lei Yu[a], Cao Xing Huang[b], Chen Huan Lai[b], Ting Ting Ma[c], Zi Shuai Zhang[a], Qiang Yong[b,*]

[a]*College of Biology and Environment, Nanjing Forestry University, Nanjing 210037, China, emails: chenrongping2000@163.com (R.P. Chen), lyu@njfu.edu.cn (L. Yu), 546452526@qq.com (Z.S. Zhang)*
[b]*College of Chemical Engineering, Nanjing Forestry University, Nanjing 210037, China, Fax: +86-25-85427045; emails: swhx@njfu.com.cn (Q. Yong), 574873906@qq.com (C.X. Huang), 451482009@qq.com (C.H. Lai)*
[c]*Key Laboratory of Soil Environment and Pollution Remediation, Institute of Soil Science, Chinese Academy of Sciences, Nanjing 210008, China, email: ttma@issas.ac.cn*

Received 12 September 2017; Accepted 22 April 2018

ABSTRACT

Magnetic humic acid nanoparticles (MHA) was prepared via coprecipitation method. Adsorptive removal of methylene blue (MB) and Cu(II) by MHA in single-component and binary systems was studied, respectively. MHA showed highly removal efficiency to MB and Cu(II). The adsorptions of MB and Cu(II) on MHA were pH dependent with uptake dropping in acidic solutions. The adsorption mechanisms of MB and Cu(II) were also different. MB is adsorbed via two mechanisms: π–π interactions and ion exchanging, while Cu(II) only involves ion exchanging. It was also proved that MHA can selectively remove MB in acidic solutions. The adsorption equilibrium and kinetic study indicated that the adsorption of MHA was in agreement with Langmuir model and pseudo-second-order model, respectively. Furthermore, MHA could be easily regenerated and reused with almost no loss of adsorption capacity. Overall, MHA is an efficient and versatile adsorbent for Cu(II) and MB.

Keywords: Humic acid; Fe_3O_4 magnetic nanoparticles; Adsorption mechanism

1. Introduction

Water contamination was becoming a global environment problem with the rapid development of the modern industries. Dye is a class of pollutants in the effluents of textile, paper, plastic, food, and cosmetic industries. The high chromaticity impedes light penetration and thus prohibits aquatic photosynthesis. Heavy metals are one of the most harmful ones due to their hazardous effects to aquatic organisms, plants, animals, and human beings in the environment. Mining, plating industries, and urban runoff are the main sources of heavy metals contamination. Therefore, both dyes and heavy metals are harmful due to their hazardous effects on aquatic biology and even human beings [1–6], it is urgent to remove these hazardous compounds from wastewater in terms of protecting public health and the environment.

Traditional treating methods for heavy metal and dye contamination removal in water, containing adsorption, ion exchange, flocculation, catalyzed degradation, filtration, biological methods, Fenton and electrochemical methods [7–15], adsorption shows multiple advantages due to its high efficiency, simple process, and reusability [16–22]. In recent years, numerous adsorbents have been developed. Among them, adsorbents prepared from natural polymers, such as cellulose, chitin, and humic acid (HA), have been paid more attentions for the advantages of eco-friendly, low cost, and wide spread [6,18,23–25]. HA is a degradation product of

* Corresponding author.

plants and animals biomass and exhibits fine reaction activity for binding multiple substances via multiple interactions (ion exchanging, chelating, and π–π interaction) [6,26].

Efficient separation of the adsorbents from water is crucial in water treatment. Sedimentation and filtration becomes cumbersome in separating adsorbents of nanometer scale. It would be very difficult to separate if the adsorbent was made into a very small size for improvement of the adsorption efficiency by increase of the surface area. Recently, magnetic separation techniques were proved to enhance the separation efficiency of small sized adsorbents [27–30]. With the aid of magnetic force, magnetic matters can be separated from the water efficiently regardless of its size. These adsorbents are in sizes of micrometer or nanometer scale. Magnetic separation techniques can bear the characteristics of large capacity, high efficiency, and small scale.

In this work, magnetic humic acid nanoparticles (MHA) were prepared by coprecipitation method and characterized by various modern analytical methods. The MHA was used for removal of two model contaminants, that is, methylene blue (MB) and Cu(II) in synthetic water samples. They were the representatives of dyes and heavy metals, respectively, which were used as model pollutants in many studies [2–6,16,18,19]. The adsorption behaviors and mechanisms of the model pollutants by MHA were systematically studied.

2. Materials and methods

2.1. Materials

HA was purchased from Aladdin Industrial Corporation (Shanghai, China). Iron(III) chloride hexahydrate, iron(II) sulfate heptahydrate, copper nitrate, ammonia solution (25%), hydrochloric acid (HCl), sodium hydroxide (NaOH), acetic acid, and MB were all supplied by Sinopharm Chemical Reagent Co. Ltd., China. All the reagents used in this work are A.R. grade. Deionized water was used in all experiments.

2.2. Preparation of adsorbent

The Fe_3O_4 and HA-coated Fe_3O_4 magnetic nanoparticles were synthesized according to the methods by Liu et al. [31]. Briefly, 12.2 g of $FeCl_3{\cdot}6H_2O$ and 8.4 g of $FeSO_4{\cdot}7H_2O$ were dissolved in 200 mL of water and heated to 90°C. Then 20 mL of ammonium hydroxide (25%) were added rapidly, followed by the addition of 100 mL of HA (1%, neutralized by NaOH). The mixture was stirred for 30 min at 90°C and then cooled to room temperature. The resultant black precipitates were collected under a magnetic field and washed to neutral with distilled water. The resultant black precipitate is MHA. Control samples, namely Fe_3O_4 nanoparticles were prepared in a similar way without HA.

2.3. Characterization of MHA

MHA underwent multiple characterizations: Fourier transform infrared spectroscopy (FTIR, on Avatar 360, Nicolet Co., USA); zeta potential analysis (on Nano ZS90, Co., UK); transmission electron microscope (TEM, on JEM-2100, JEOL Co., Japan); thermogravity analysis (TG, on STA-449C, Netzsch Instrument Co. Ltd., Germany); vibrating sample magnetometer (on MPMS-XL7, Quantum Design, USA); and X-ray diffraction (XRD, Ultima IV, Rigaku Co. Ltd., Japan).

2.4. MB and Cu(II) removal in respective single-component systems

The adsorption behavior of MHA in the removal of MB and Cu(II) in their respective single-component systems was studied.

The concentration of MB was analyzed by a Victor 722 Vis Spectrometer at 662 nm. Cu(II) concentration was analyzed by a Thermo Fisher ICE 3500 atomic absorption spectrophotometer. Prior to each measurement, proper dilution was performed if necessary to ensure that the concentration of the sample was within the range of the standard curves.

2.4.1. Effect of initial solution pH

The initial pH ranges of the solutions were 1.84–6.06 for Cu(II) and 2.0–10.2 for MB. The upper pH limit of Cu(II) was set to avoid the precipitation of metal hydroxide. The initial concentration of MB and Cu(II) in solutions was all 400 mg/L, based on adsorption isotherms. In the adsorption experiments, MHA sample was added MB and Cu(II) solutions with different initial pH values and stirred for 24 h for equilibrate. The mass of MHA is 0.05 g and the volume of each solution is 50 mL.

2.4.2. Adsorption equilibrium study

Adsorption equilibrium study was conducted at pH 6.07. 0.08 g of MHA was dosed in 80 mL of Cu/MB solutions with the initial concentrations from 10 to 200 mg/L under continuous stirring. Adsorption capacity was calculated according to Eq. (1).

$$q_e = \frac{(C_0 - C_e)V}{m} \tag{1}$$

where C_0 and C_e (mg/L) are the initial and equilibrium MB or Cu(II) concentrations in solution, respectively, V (L) is the volume of solution, and m (g) is the weight of dry adsorbents.

The adsorption equilibrium data were simulated by Langmuir and Freundlich model.

Langmuir model is based on the assumption of a monolayer adsorption on a homogeneous surface [32]. The equation is expressed in Eq. (2) as follows:

$$\frac{C_e}{q_e} = \frac{1}{q_m b} + \frac{C_e}{q_m} \tag{2}$$

where q_e (mg/g) is the amount of Cu(II) and MB adsorbed at equilibrium, C_e (mg/L) is the Cu(II) and MB concentration at equilibrium, q_m (mg/g) is the maximum adsorption capacity when an adsorbent is fully covered, and b (L/mg) is the Langmuir adsorption constant which relates to the adsorption energy.

Freundlich model assumes multilayer adsorption with sites of exponentially distribute adsorption energies. It is expressed in Eq. (3) as follows [33]:

$$\ln\left(q_e\right) = \ln\left(K_f\right) + \frac{1}{n}\ln\left(C_e\right) \tag{3}$$

where K_f is the Freundlich isotherm constant and n (dimensionless) is the heterogeneity factor. C_e is the equilibrium concentration (mg/L), and q_e is the amount of MB or Cu(II) adsorbed at equilibrium (mg/g).

The thermodynamic parameters are calculated based on the fundamental thermodynamic Eqs. (4) and (5) as follows [34]:

$$\Delta G = -RT\ln(bM) \tag{4}$$

$$\Delta G = \Delta H - T\Delta S \tag{5}$$

where b is the thermodynamic distribution coefficient obtained from Langmuir model (L/mg), M (mg/mol) is the molecular weight of the adsorbate, R is the universal gas constant (8.314 J/(mol K)), T is the temperature (K), ΔG (kJ/mol) is Gibbs free energy, ΔH (kJ/mol) is the enthalpy change, and ΔS (J/(mol K)) is the entropy change in the process.

2.4.3. Adsorption kinetics study

Kinetic adsorption experiments were performed at 298 K and initial pH 6.07. The initial concentration of MB and Cu(II) solution was the same as in Section 2.4.1. About 0.5 g of adsorbent was immerged into 500 mL MB or Cu(II) solution under continuous agitation. Then, 1 mL of sample solutions was taken out at certain time intervals to measure the current concentrations. Meanwhile, the same volume of pure water was added into the bulk solution to keep the volume constant. The dye or metal uptake $q(t_i)$ (mg/g) at time t_i was calculated using the Eq. (6) as follows:

$$q(t_i) = \frac{(C_0 - C_{t_i})V_0 - \sum_2^{i-1} C_{t_{i-1}} V_a}{m} \tag{6}$$

where C_0 and C_{t_i} (mg/L) are the initial dye or metal concentration and its concentrations at time t_i, respectively. V_0 and V_a (L) are the volume of the mixed solution and the volume of the sample solution taken out at t_i for analysis, respectively. In this case, V_a equals to 1.0 mL and m (g) represents the weight of the adsorbent. The kinetics data were simulated by the pseudo-first-order kinetic, the pseudo-second-order kinetic, and the intraparticle diffusion model [35,36].

The pseudo-first-order kinetic model was shown in Eq. (7) as follows:

$$\ln(q_e - q_t) = \ln q_e - k_1 t \tag{7}$$

where k_1 (min^{-1}) is the rate constant of pseudo-first-order adsorption, q_e and q_t (mg/g) are the amount of Cu(II) or MB absorbed onto adsorbents at equilibrium and at time t (min), respectively.

The pseudo-second-order kinetic model is expressed in Eq. (8) as follows:

$$\frac{t}{q_t} = \frac{1}{k_2 q_e^2} + \frac{t}{q_e} \tag{8}$$

where q_e and q_t (mg/g) are the amounts of Cu(II) or MB adsorbed onto adsorbents at equilibrium and at time t (min), respectively, k_2 (g/(mg min)) is the rate constant of pseudo-second-order model.

Intraparticle diffusion model suggests that intraparticle diffusion is the rate-limiting step in the adsorption. The model is shown in Eq. (9) as follows:

$$q_t = k_p t^{0.5} + c \tag{9}$$

where k_p (mg/(g $min^{0.5}$)) is the intraparticle diffusion rate constant and c (mg/g) is the intercept of this equation.

The activation energy of the adsorption was calculated based on Arrhenius equation, which is expressed as follows [36]:

$$\ln k_2 = -\frac{E_a}{RT} + \ln(A) \tag{10}$$

where k_2 is the rate constant of pseudo-second-order adsorption (g/(mg·min)), as the adsorption kinetics follow this model, E_a is the activation energy of adsorption (kJ/mol), A is the Arrhenius factor, R is the universal gas constant (8.314 J/(mol K)), T is the temperature (K).

2.5. MB and Cu(II) removal in a binary system

The adsorption of Cu/MB in a binary system was carried out at 298 K. The effect of initial solution pH and adsorption kinetic was studied, the experimental conditions were similar to those conducted in Section 2.4, except that the solution consist of MB/Cu(II) with equal initial concentration.

2.6. Recycling experiment

In this experiment, 0.1 mol/L EDTA solution was selected as the regeneration agent to recover the used adsorbents. The recovered adsorbent was then reactivated by 0.1 mol/L of NaOH solution and subsequently washed with distilled water. The regenerated adsorbent was reused in the next adsorption–regeneration cycle and conducted for five cycles. The adsorption capacity of MHA in the first cycle is set as 100% and the recycle efficiency (%) of regenerated MHA equals the ratio of the adsorption capacity in the current cycle to the capacity in the first cycle.

3. Results and discussion

3.1. Characterization of MHA

FTIR spectra of MHA, Fe_3O_4, and HA are shown in Fig. 1. For Fe_3O_4 and MHA, the peak at 582 cm^{-1} corresponds to the characteristic stretching vibration of the Fe–O bond [26,31,37]. The band at 1,630 cm^{-1} of MHA is ascribed to the C=O stretching band, indicating the carboxylate anion interaction with the ferroxide surface [26,31]. The band at 1,400 cm^{-1} can be ascribed to CH_2 scissoring [38]. The band at 1,110 cm^{-1} is the C–O stretching of COO^-. Previous studies indicate that the binding of HA to Fe_3O_4 surface was mainly achieved through coordination [31]. It can be concluded that the carboxylate groups interacted with FeO surface and played an important role in the bonding of the HA with the magnetite surface.

Zeta potentials of the MHA were measured at various pH and are shown in Fig. 2. As shown in Fig. 2, it is observed that the isoelectric point of MHA is approximately at pH 3.2 which may be due to the carboxyl groups on HA coating [39].

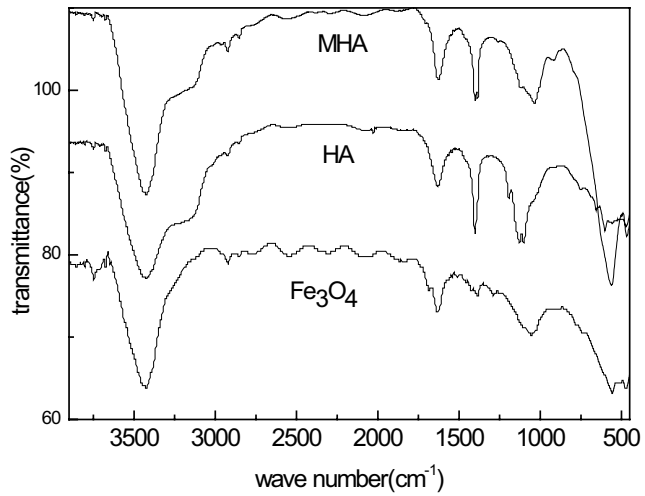

Fig. 1. FTIR spectra of MHA, Fe_3O_4, and HA.

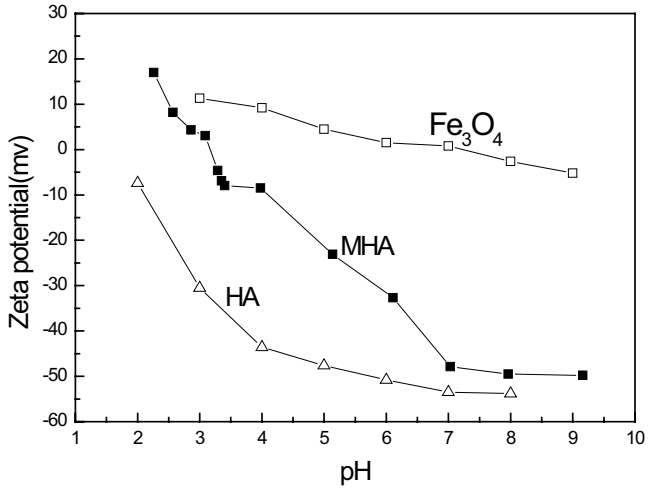

Fig. 2. Zeta potential curve of MHA, Fe_3O_4, and HA at different initial solution pH.

The zeta potential of HA is negative in the pH range of 2–9 and the zeta potential of Fe_3O_4 is positive below pH 7 and negatively above the point according to Fig. 2. The zeta potential plot of MHA suggests that HA is coated on Fe_3O_4 surfaces. It also indicated that MHA is negatively charged at the environment of pH 3.2–9.5, which impedes the aggregation of MHA nanoparticles and is also beneficial for the adsorption of cationic species. Illes and Tombacz [39] indicated that the colloidal stability of Fe_3O_4 nanoparticles coated with HA in aqueous solution is enhanced.

As shown in Fig. 3, the saturation magnetization of MHA and Fe_3O_4 is 62.88 and 69.58 emu/g, respectively. The relatively high magnetization value makes the separation of MHA from its aqueous dispersions under an external magnetic field easy. MHA can quickly aggregate in the magnetic field and then achieve separation.

It is observed from Fig. 4 that the MHA has a quasispherical structure feature with particle size of about 10 nm. The TG curve of MHA was shown in Fig. 5, the weight loss at 350°C is due to decomposition, dehydration, and carbonization of

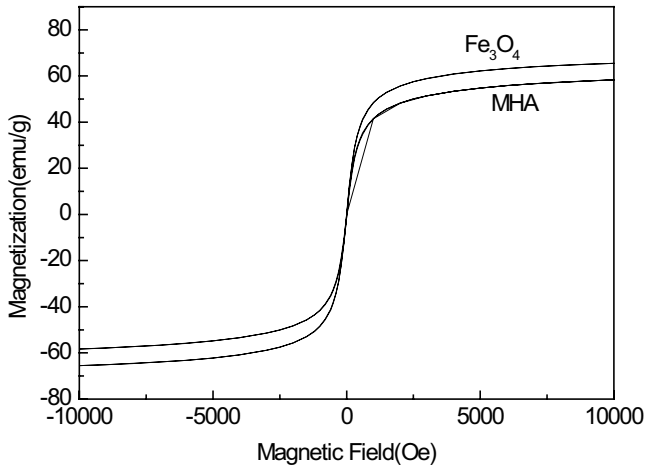

Fig. 3. Magnetization curves of MHA and Fe_3O_4.

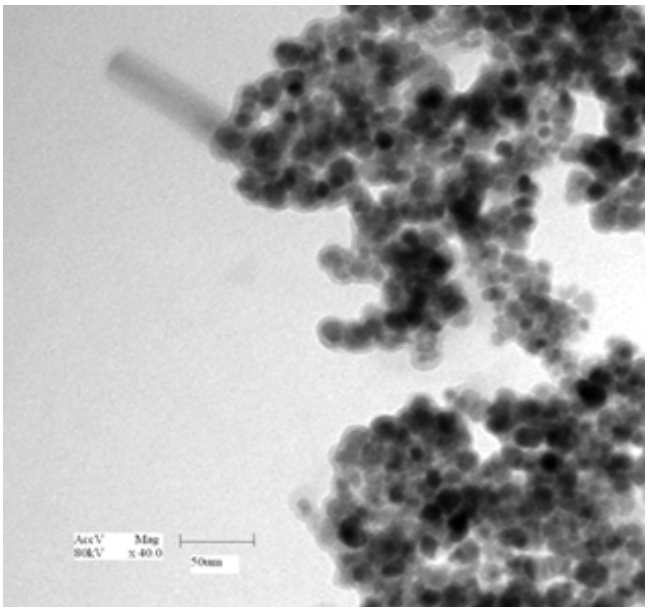

Fig. 4. TEM image of MHA nanoparticles.

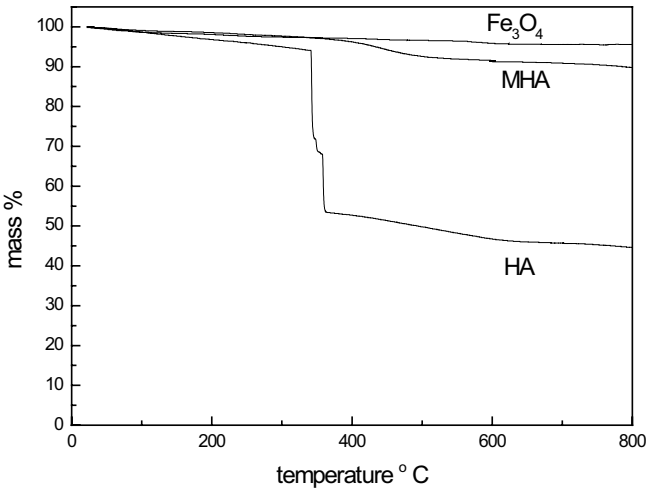

Fig. 5. TG curves of Fe_3O_4, MHA, and HA.

HA. As the weight loss of Fe_3O_4 is rather small, it is neglected for calculation convenience. The content of HA in MHA is calculated based on the ratio of HA weight loss and MHA weight loss. According to the curve, MHA contains about 18% HA.

XRD patterns of pristine Fe_3O_4 and MHA are shown in Fig. 6. The two samples of pristine Fe_3O_4 and MHA have similar characteristic diffraction peaks at 2θ = 30.3°, 35.4°, 42.6°, 53.9°, 57.2°, and 62.8°, which correspond to the characteristic (220), (311), (400), (422), (511), and (440) planes of cubic Fe_3O_4 phase with a spinel structure (JCPDS No. 85-1436) [38]. There is no distinct difference between the nanoparticles of Fe_3O_4 and MHA, indicating that the crystal structure of Fe_3O_4 in MHA is maintained after coating with HA.

3.2. Removal of MB and Cu(II)

3.2.1. Effect of initial solution pH

The plots of adsorption capacity versus initial pH are shown in Fig. 7(a). The upper limit of studied pH of MB and Cu(II) was set at about 9 and 6, respectively. As shown in Fig. 7(a), the adsorption of MB and Cu(II) was strongly pH-dependent and there are two stages in the curve of MB. For MB, the optimal pH range was about 6–9, where the adsorption capacity was about 200 mg/g. The adsorption of MHA to MB in the initial solution pH range of 4–6 was mainly due to carboxyl groups, while in the pH range of 6–9 was due to the carboxyl and phenolic hydroxyl groups together. For Cu(II), the optimal pH range was 4–6, with a maximal adsorption capacity of about 57 mg/g. Compared with Fe_3O_4 nanoparticles, the adsorption capacity of MHA for both MB and Cu(II) was about 16 times higher than the value of Fe_3O_4.

In acidic solutions, the adsorption capacity of MB and Cu(II) was all dropped, but MB still retained part of the adsorption while the uptake of Cu(II) is barely above zero. This is due to the protonation of the anionic groups on MHA, which are weakly acidic. The adsorption difference in acidic solutions is due to the different adsorption mechanism of the two type contaminants. Cu(II) mainly binds with anionic groups, which is easily protonated by acids [6,35], while MB can bind with both anionic and aromatic groups of MHA through ion exchange and π–π interaction, respectively. Because π–π interaction is pH independent, MHA can still adsorb MB in acidic conditions.

To further investigate the adsorption mechanism and contaminant interaction, we carried out the adsorption experiments in a binary system. As shown in Fig. 7(b), there is an obvious competition between the two contaminants in near neutral solutions, where the adsorption of MB dropped about half and the adsorption of Cu(II) dropped about 30%. In acidic solutions, the uptakes of both contaminants were close to those in single systems. The competition in neutral solution can be attributed to anionic groups, and in acidic solutions the competition vanished with the protonation of those groups [6]. According to the drop in adsorption capacity in near neutral solutions, the affinity of Cu(II) on anionic groups is higher than MB, as its uptake was better retained. Because MB can interact with aromatic groups on MHA, the total adsorption capacity of MB was still higher than Cu(II). By interacting with aromatic groups, MB can also retain part of its adsorption in strongly acidic solutions, where the

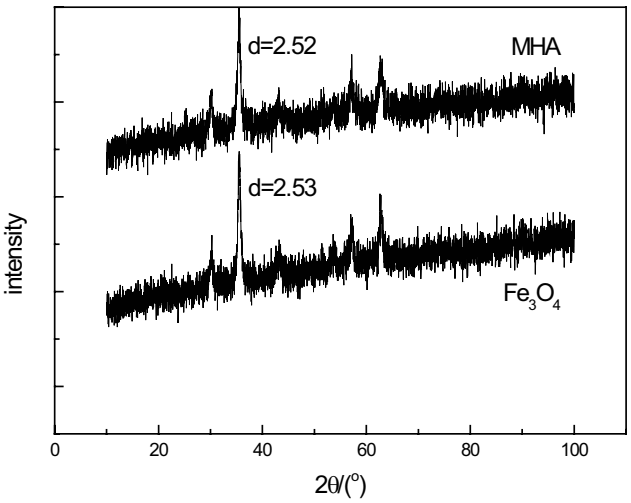

Fig. 6. XRD patterns of Fe_3O_4 and MHA.

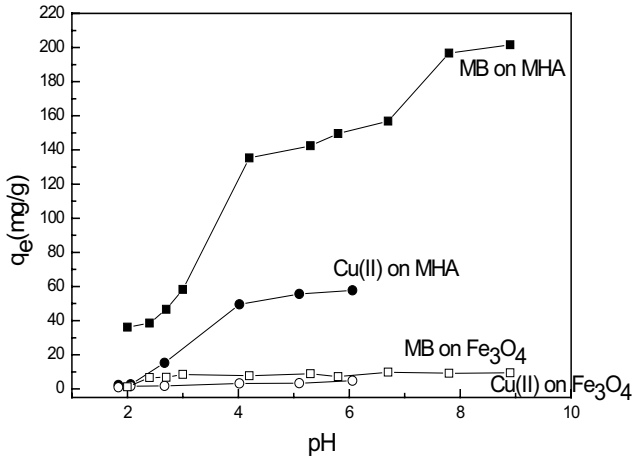

(a)

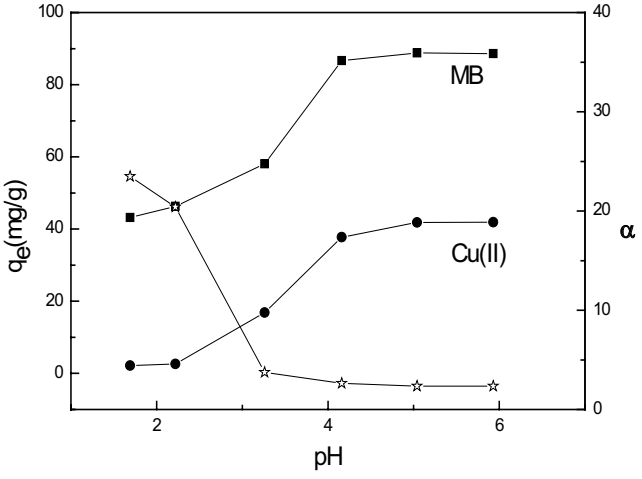

(b)

Fig. 7. The effect of initial solution pH on the adsorption of Cu(II) and MB at 298 K: (a) single system; (b) binary system.

anionic groups are no longer available. It can also indicate that in acidic solutions, MHA shows conditional adsorption selectivity toward MB, and the adsorbed Cu(II) can be separated from coadsorbed MB. The results of binary system further confirmed the adsorption mechanism. The π–π binding adsorption of MHA with aromatic compounds also indicated that MHA may have application potential for the remediation of aromatic pollutants.

To quantitatively evaluate the preference of MHA for Cu(II) and MB, the selectivity coefficient (α) in the binary system was calculated. The term α is defined by Eq. (11) [6].

$$\alpha = \frac{\left(C_{01} - C_{e1}\right)C_{e2}}{C_{e1}\left(C_{02} - C_{e2}\right)} \cdot \frac{V_1 m_2}{m_1 V_2} \tag{11}$$

where C_{0x} and C_{ex} (mg/L) are the initial and equilibrium concentrations of component x in solution, respectively; V (L) is the volume of solution; m (g) is the weight of adsorbents.

As illustrated in Fig. 7(b), the α values were kept at high level in the acidic solutions. It is because that available anionic sites for Cu(II) are deactivated by protonation, while MB can still be adsorbed by the unaffected aromatic sites [6]. The higher α values confirmed the conditional selectivity aforementioned. As the solution changes from acidic to neutral, the α begins to fall from about 23 to 2, indicating almost no selectivity in neutral solutions. The fall is due to the reactivation of anionic groups on MHA, which is more favorable to Cu(II) than MB.

3.2.2. Adsorption equilibrium study

The equilibrium isotherm is fundamental to describe the interactive behaviors between the solutes and adsorbents and illuminate the properties and affinity of the adsorbent.

The adsorption isotherms at three temperatures were measured and the results are shown in Fig. 8. The adsorptions of Cu(II) and MB were increased almost linearly with the initial concentrations at the beginning, then reached to surface saturation at high concentrations. It indicated that, at lower initial concentrations of Cu(II) and MB, the adsorption sites on the adsorbents were sufficient and the Cu(II) and MB uptakes relied on the amount of Cu(II) and MB transported from the bulk solution to the surfaces of the adsorbents. However, at higher initial concentrations, the adsorption sites on the MHA surfaces were saturated, and the adsorption achieved equilibrium. The adsorption capacities of Cu(II) and MB increase with increasing temperature, indicating more favorable adsorption at higher temperature.

To evaluate the adsorption behavior of MHA, the experimental data were analyzed by Langmuir and Freundlich model. Langmuir model is based on the assumption that adsorption sites are identical and energetically equivalent, only monolayer adsorption occurs in the process [32]. Freundlich isotherm model is based on the assumption of an exponentially decaying adsorption site energy distribution [33].

The simulation results are listed in Tables 1(a) and (b). The correlation coefficients (R^2) of Langmuir model were higher than those of Freundlich at all the temperatures. And the q_m calculated from Langmuir model at each temperature is closer to the experimental data. So the isothermal adsorption behaviors of MB and Cu(II) on MHA follow Langmuir equation and are monolayer processes.

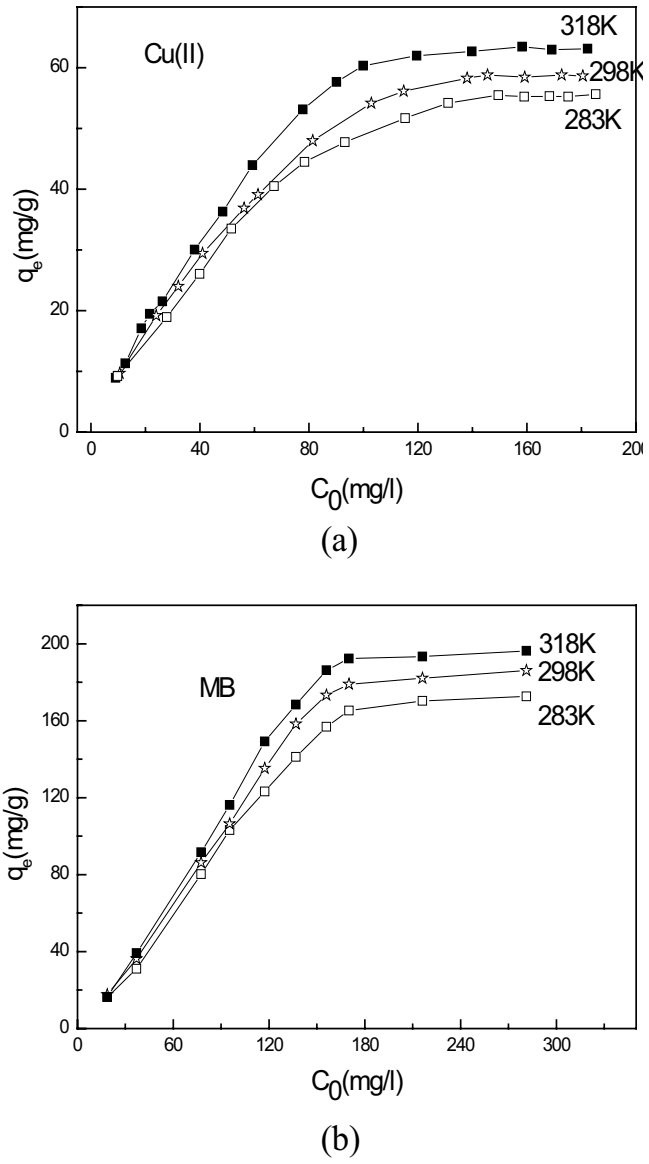

Fig. 8. The isothermal equilibrium adsorption plots of Cu(II) (a) and MB (b) at 283, 298, and 318 K.

Table 1(a)
Isothermal parameters for the adsorption of MB on MHA based on Langmuir and Freundlich models at 283, 298, and 318 K with initial pH 6.07

Model	Parameter	Temperature (K)		
		283	298	318
Langmuir	q_m (mg/g)	200	200	200
	b (L/mg)	1.67	2.50	1.67
	R^2	0.99	0.99	0.99
Freundlich	K_F	7.40	7.57	7.13
	n	3.77	3.88	4.27
	R^2	0.64	0.54	0.68

Table 1(b)
Isothermal parameters for the adsorption of Cu(II) on MHA based on Langmuir and Freundlich models at 283, 298, and 318 K with initial pH 6.07

Model	Parameter	Temperature (K)		
		283	298	318
Langmuir	q_m (mg/g)	62.50	66.67	71.43
	b (L/mg)	0.07	0.08	0.14
	R^2	0.99	0.99	0.99
Freundlich	K_F	10.97	11.11	14.38
	n	2.81	2.65	2.87
	R^2	0.95	0.97	0.95

Table 2(a)
Thermodynamic parameters for the adsorption of MB onto MHA at 283, 298, and 318 K with initial pH 6.07

ΔH (kJ/mol)	ΔS (J/mol K)	ΔG (kJ/mol)		
–7.77	87	283 K	298 K	318 K
		−31.39	−34.07	−35.27

Table 2(b)
Thermodynamic parameters for the adsorption of Cu onto MHA at 283, 298, and 318 K with initial pH 6.07

ΔH (kJ/mol)	ΔS (J/mol K)	ΔG (kJ/mol)		
15.79	125.30	283 K	298 K	318 K
		−19.85	−21.28	−24.19

The thermodynamic parameters are listed in Tables 2(a) and (b). The values of ΔG of MB and Cu(II) at all the temperatures are negative, indicating spontaneous adsorption at these temperatures. The values of ΔS of MB and Cu(II) are positive, suggesting that the adsorption is a process with entropy increase.

3.2.3. Adsorption kinetics study

The kinetic adsorption results of MB and Cu(II) on MHA are shown in Fig. 9. It is observed that the adsorption equilibrium was achieved in about 15 min for MB and about 20 min for Cu(II), which were both satisfactory in the practical application.

In order to investigate the adsorption mechanism further, the data were simulated according to three kinetic models: pseudo-first-order model, pseudo-second-order, and intraparticle diffusion model.

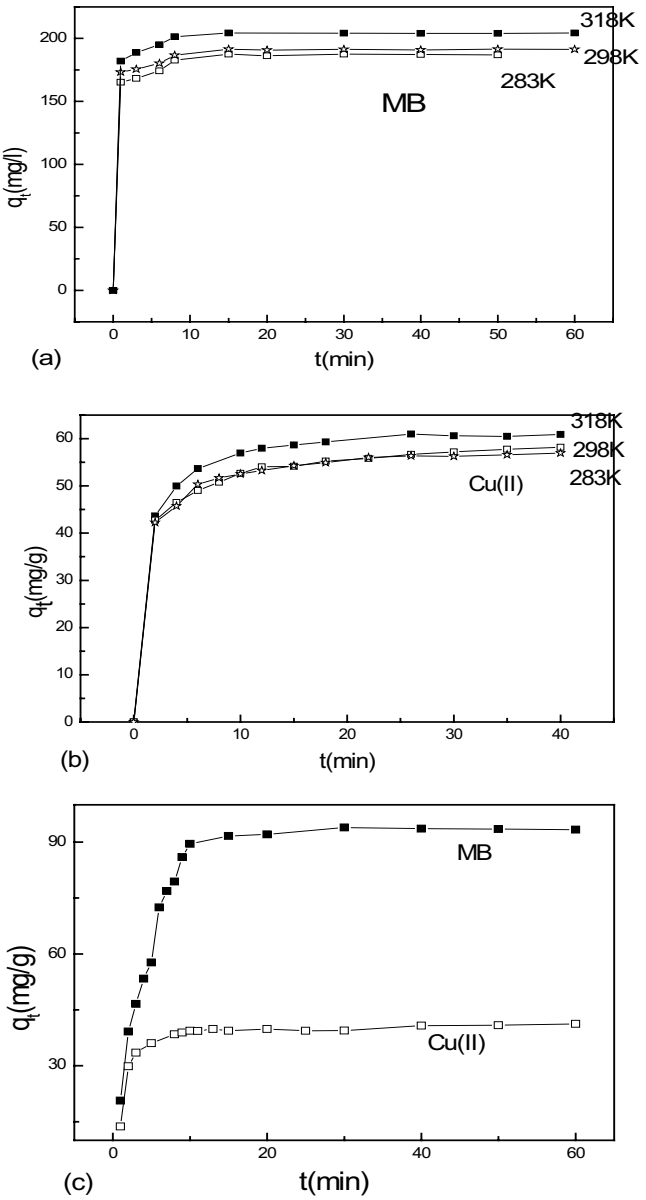

Fig. 9. The adsorption kinetic plots of MB (a) and Cu(II) (b) at 283, 298, 318 K, and a binary system of both adsorbates (c).

The results are listed in Tables 3(a) and (b). Based on the various kinetic models, the correlation coefficient (R^2) of pseudo-second-order model is higher than the other models, and the

Table 3(a)
Kinetic parameters for MB onto MHA at 283, 298, and 318 K with initial pH 6.07

T (K)	$q_{e,\exp}$ (mg/g)	Pseudo-first-order model			Pseudo-second-order model			Intraparticle diffusion model		
		k_1 (min^{-1})	$q_{e,\text{cal}}$ (mg/g)	R^2	k_2 (g/mg min)	$q_{e,\text{cal}}$ (mg/g)	R^2	k_p (mg/g min$^{0.5}$)	C (mg/g)	R^2
283	187.57	0.059	22.97	0.952	0.021	188.32	0.999	1.56	142.41	0.934
298	191.39	0.052	23.08	0.989	0.025	192.31	0.999	2.86	142.85	0.989
318	204.32	0.042	24.56	0.885	0.029	204.92	0.999	2.14	143.22	0.941

Table 3(b)
Kinetic parameters for Cu(II) onto MHA at 283, 298, and 318 K with initial pH 6.07

T (K)	$q_{e,exp}$ (mg/g)	Pseudo-first-order model			Pseudo-second-order model			Intraparticle diffusion model		
		k_1 (min^{-1})	$q_{e,cal}$ (mg/g)	R^2	k_2 (g/mg min)	$q_{e,cal}$ (mg/g)	R^2	k_p (mg/g min$^{0.5}$)	C (mg/g)	R^2
283	56.95	0.158	17.32	0.978	0.016	58.83	0.999	5.98	37.17	0.930
298	58.17	0.185	20.39	0.986	0.017	58.83	0.999	3.65	39.64	0.923
318	60.91	0.192	21.85	0.993	0.018	62.50	0.999	1.66	47.27	0.919

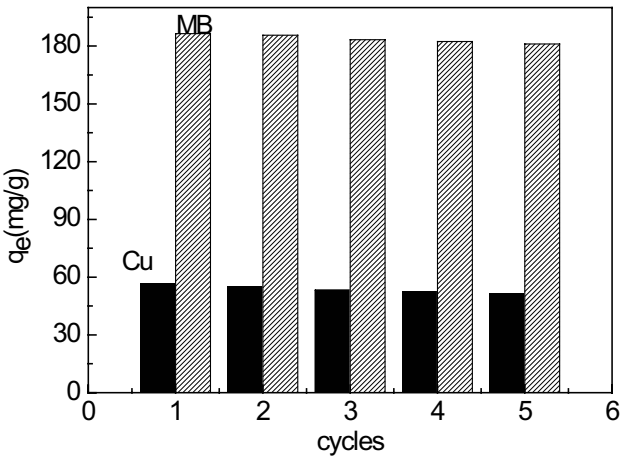

Fig. 10. Variation on adsorption capacity in regeneration cycles of MB and Cu(II).

theoretical q_e values are also closer to the experimental ones, pseudo-second-order kinetic model is more appropriate to describe the adsorption kinetics behaviors for MB and Cu onto the MHA.

Based on Arrhenius equation, a plot of lnk_2 versus $1/T$ yields a straight line, with slope$-E_a/R$. The value of E_a can be used to differentiate physical and chemical adsorptions. The activation energy of Cu(II) and MB is 2.51 and 6.02 kJ/mol, respectively, indicating that the adsorption is physical one. It also confirms the adsorption equilibrium time of MB is shorter than Cu(II).

We also carried out kinetic study in binary system to investigate the effect of competition on adsorption rate. As shown in Fig. 9(c), there was a drop of adsorption capacity of Cu(II) and MB. However, the rate of adsorption was not significantly affected by the competition of the adsorbates, indicating that the time efficiency of MHA in the binary system is as high as in the single ones.

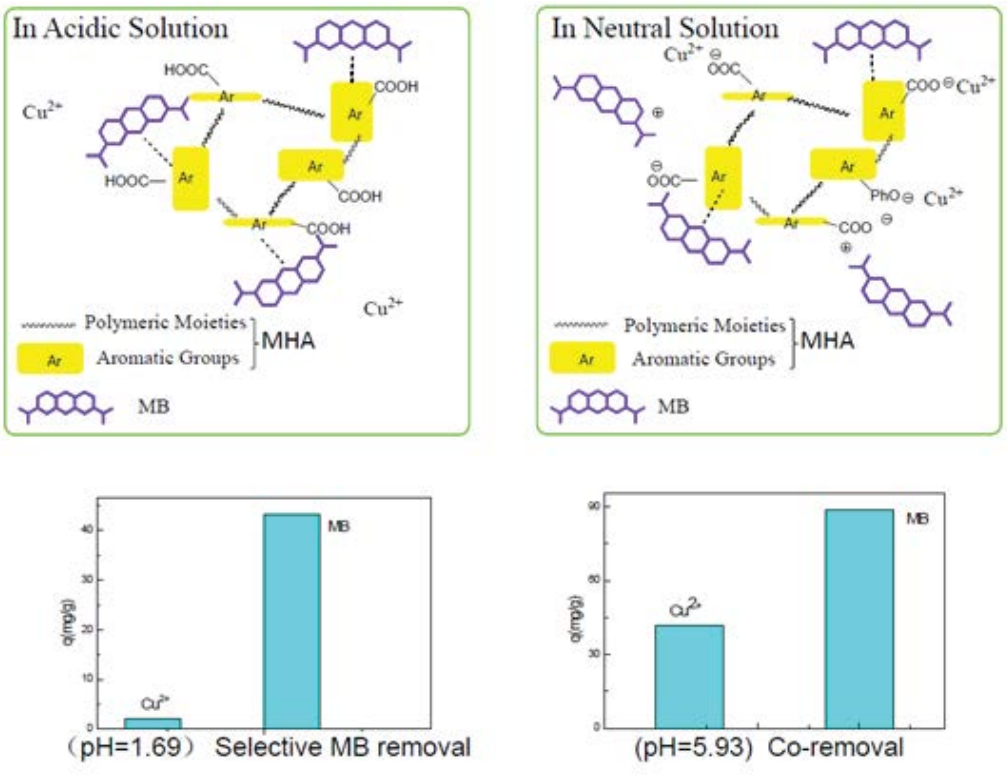

Fig. 11. The adsorption mechanism of MB and Cu(II) on MHA.

3.3. Reuse of MHA

The regeneration results are shown in Fig. 10. The adsorption capacity of MB and Cu(II) only experienced very slight drops (<5%) after five cycles. It suggested that the reusability of MHA is satisfactory for practical applications.

4. Conclusion

In this work, MHA was prepared using coprecipitation method. MHA showed high removal efficiency for MB and Cu(II) and fine magnetic response. The adsorption mechanism of MB and Cu(II) was illustrated in Fig. 11. As shown in Fig. 11, the adsorption of Cu(II) mainly occurred on anionic groups on MHA while the adsorption of MB took place on both anionic and aromatic groups, since it is an aromatic compound. The adsorption of MB and Cu(II) on MHA was pH-dependent due to the pH-sensitivity of the anionic groups on MHA, which played major roles in the adsorption in neutral solutions. The pH-dependency of MB less notable than Cu(II) was due to its ability to interact with MHA through π–π interactions, which make MHA can separate MB from Cu(II) in acidic solutions. The adsorption of MB and Cu(II) was monolayer and the adsorption kinetics was in agreement with the pseudo-second-order equation. The adsorption was all physical processes according to the value of activation energy (E_a). Besides, the adsorbent can be easily regenerated and efficiently reused after a few cycles.

Acknowledgments

This work was supported by Natural Science Foundation of Jiangsu provincial universities (17KJB220006), the Priority Academic Program Development of Jiangsu Higher Education Institutions (PAPD), and Science and Technology Program of Jiangsu, China (SBK2014043721).

References

[1] J. Li, China gears up to tackle tainted water, Nature, 499 (2013) 14–15.
[2] Z. Xu, G.D. Gao, B.C. Pan, A new combined process for efficient removal of Cu(II) organic complexes from wastewater: Fe(III) displacement/UV degradation/alkaline precipitation, Water Res., 87 (2015) 378–384.
[3] M. Solís, A. Solís, H.I. Pérez, Microbial decolorization of azo dyes: a review. Process Biochem., 47 (2012) 1723–1748.
[4] L.C. Fang, P. Cai, P.X. Li, Microcalorimetric and potentiometric titration studies on the adsorption of copper by *P. putida* and *B. thuringiensis* and their composites with minerals, J. Hazard. Mater., 181 (2010) 1031–1038.
[5] P.K. Rai, Heavy metal pollution in aquatic ecosystems and its phytoremediation using wetland plants: an ecosustainable approach, Int. J. Phytorem., 10 (2008) 133–160.
[6] R.P. Chen, Y.L. Zhang, L.F. Shen, Lead (II) and methylene blue removal using a fully biodegradable hydrogel based on starch immobilized humic acid, Chem. Eng. J., 268 (2015) 348–355.
[7] M. Hunsom, K. Pruksathorn, S. Damronglerd, H. Vergnes, P. Duverneuil, Electrochemical treatment of heavy metals (Cu^{2+}, Cr^{6+}, Ni^{2+}) from industrial effluent and modeling of copper reduction, Water Res., 39 (2005) 610–616.
[8] C.D. Shuang, P.H. Li, A.M. Li, Quaternized magnetic microspheres for the efficient removal of reactive dyes, Water Res., 46 (2012) 4417–4426.
[9] G.S. Simate, S.E. Iyuke, S. Ndlovu, The heterogeneous coagulation and flocculation of brewery wastewater using carbon nanotubes, Water Res., 4 (2012) 1185–1197.
[10] S. Anandan, P.S. Kumar, N. Pugazhenthiran, Effect of loaded silver nanoparticles on TiO_2 for photocatalytic degradation of acid red 88, Sol. Energy Mater. Sol. Cells, 92 (2008) 929–937.
[11] L. Yu, W.W. Li, M.H.W. Lam, Isolation and characterization of a *Klebsiella oxytoca* strain for simultaneous azo-dye anaerobic reduction and bio-hydrogen production, Appl. Microbiol. Biotechnol., 95 (2012) 255–262.
[12] A. Özcan, M. Gençten, Investigation of acid red 88 oxidation in water by means of electro-Fenton method for water purification, Chemosphere, 146 (2016) 245–252.
[13] T. Robinson, B. Chandran, P. Nigam, Effect of pretreatments of three waste residues, wheat straw, corncobs and barley husks on dye adsorption, Bioresour. Technol., 85 (2002) 119–124.
[14] N.K. Srivastava, C.B. Majumder, Novel biofiltration methods for the treatment of heavy metals from industrial wastewater, J. Hazard. Mater., 151 (2008) 1–8.
[15] S. Hsu, P.C. Singer, Removal of bromide and natural organic matter by anion exchange, Water Res., 44 (2010) 2133–2140.
[16] F. Ferrero, Adsorption of methylene blue on magnesium silicate: kinetics, equilibria and comparison with other adsorbents, J. Environ. Sci., 22 (2010) 467–473.
[17] Q. Huang, M.Y. Liu, J.Y. Chen, Facile preparation of MoS_2 based polymer composites via mussel inspired chemistry and their high efficiency for removal of organic dyes, Appl. Surf. Sci., 419 (2017) 35–44.
[18] M. Rafatullah, O. Sulaiman, R. Hashim, A. Ahmad, Adsorption of methylene blue on low-cost sorbents: a review, J. Hazard. Mater., 177 (2010) 70–80.
[19] B.H. Hameed, A.T.M. Din, A.L. Ahmad, Sorption of methylene blue onto bamboo-based activated carbon: kinetics and equilibrium studies, J. Hazard. Mater., 141 (2007) 819–825.
[20] R. Jiang, Y.Q. Fu, H.Y. Zhu, Removal of methyl orange from aqueous solutions by magnetic maghemite/chitosan nanocomposite films: adsorption kinetics and equilibrium, J. Appl. Polym. Sci., 125 (2012) 540–549.
[21] G. Crini, Studies on adsorption of dyes on beta-cyclodextrin polymer, Bioresour. Technol., 90 (2003) 193–198.
[22] D.D. Asouhidou, K.S. Triantafyllidis, N.K. Lazaridis, Adsorption of Remazol Red 3BS from aqueous solutions using APTES- and cyclodextrin-modified HMS-type mesoporous silicas, Colloids Surf., A, 346 (2009) 83–90.
[23] J. Lin, Y. Zhan, Adsorption of humic acid from aqueous solution onto unmodified and surfactant-modified chitosan/zeolite composites, Chem. Eng. J., 200 (2012) 202–213.
[24] T.S. Anirudhan, C.D. Bringle, S. Rijith, Removal of uranium(VI) from aqueous solutions and nuclear industry effluents using humic acid-immobilized zirconium-pillared clay, Desal. Wat. Treat., 12 (2009) 16–27.
[25] J. Hizal, R. Apak, Modeling of cadmium(II) adsorption on kaolinite-based clays in the absence and presence of humic acid, Appl. Clay Sci., 32 (2006) 232–244.
[26] L. Carlos, M. Cipollone, D.B. Soria, The effect of humic acid binding to magnetic nanoparticles on the photogeneration of reactive oxygen species, Sep. Purif. Technol., 91 (2012) 23–29.
[27] H. Yang, B. Yuan, Y.B. Lu, R.S. Cheng, Preparation of magnetic chitosan microspheres and its applications in wastewater treatment, Sci. China, Ser. B, 52 (2009) 249–256.
[28] Y.X. Huang, A. Keller Arturo, EDTA functionalized magnetic nanoparticle sorbents for cadmium and lead contaminated water treatment, Water Res., 80 (2015) 159–168.
[29] R.P. Chen, Y.L. Zhang, X.Y. Wang, Removal of methylene blue from aqueous solution using humic-acid coated magnetic nanoparticles, Desal. Wat. Treat., 55 (2015) 539–548.
[30] W.P. Liu, J.Q. Ma, C.S. Shen, A pH-responsive and magnetically separable dynamic system for efficient removal of highly dilute antibiotics in water, Water Res., 90 (2016) 24–33.
[31] J.F. Liu, Z.S. Zhao, G.B. Jiang, Coating Fe_3O_4 magnetic nanoparticles with humic acid for high efficient removal of heavy metals in water, Environ. Sci. Technol., 42 (2008) 6949–6954.

[32] I. Langmuir, The adsorption of gases on plane surfaces of glass, mica and platinum, J. Am. Chem. Soc., 40 (1918) 1361–1402.
[33] H.M.F. Freundlich, Ueber die Adsorption in Loesungen, Z. Phys. Chem., 57 (1906) 385–470.
[34] H.K. Boparai, M. Joseph, D.M. O'Carroll, Kinetics and thermodynamics of cadmium ion removal by adsorption onto nanozerovalent iron particles, J. Hazard. Mater., 186 (2011) 458–465.
[35] J. Dai, H. Yan, H. Yang, Simple method for preparation of chitosan/poly(acrylic acid) blending hydrogel beads and adsorption of copper(II) from aqueous solutions, Chem. Eng. J., 165 (2010) 240–249.
[36] H. Yan, H.J. Li, X. Tao, Rapid removal and separation of Iron(II) and manganese(II) from micropolluted water using magnetic grapheme oxide, ACS Appl. Mater. Interfaces, 6 (2014) 9871–9880.
[37] R.A. Alvarez-Puebla, J.J. Garrido, Effect of pH on the aggregation of a gray humic acid in colloidal and solid states, Chemosphere, 59 (2005) 659–667.
[38] S.T. Yang, P.F. Zong, X.M. Ren, Rapid and high-efficient preconcentration of Eu by core-shell structured Fe_3O_4@humic acid magnetic nanoparticles, ACS Appl. Mater. Interfaces, 12 (2012) 6890–6899.
[39] E. Illes, E. Tombacz, The effect of humic acid adsorption on pH-dependent surface charging and aggregation of magnetite nanoparticles, J. Colloid Interface Sci., 295 (2006) 115–123.